

Longitudinal Relaxation (T_1) of Methane/Hydrogen Mixtures for *Operando* Characterization of Gas-Phase Reactions

Harm Ridder,* Christoph Sinn, Georg R. Pesch, Wolfgang Dreher, and Jorg Thöming

Cite This: *ACS Meas. Sci. Au* 2022, 2, 449–456

Read Online

ACCESS |



Metrics & More



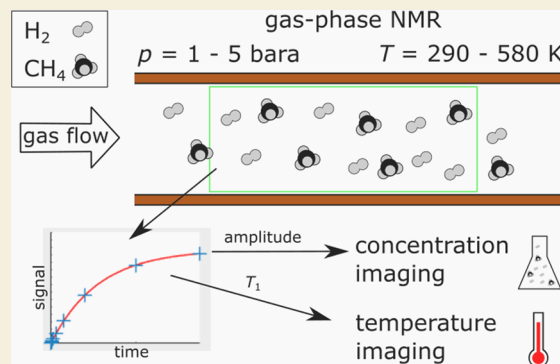
Article Recommendations



Supporting Information

ABSTRACT: Catalytic hydrogenation reactions are important in a modern hydrogen-based society. To optimize these gas-phase reactions, a deep understanding of heat, mass, and momentum transfer inside chemical reactors is required. Nuclear magnetic resonance (NMR) measurements can be used to obtain spatially resolved values of temperature, gas composition, and velocity in the usually opaque catalytic macrostructures. For this, the desired values are calculated from measured NMR parameters like signal amplitude, T_1 , or T_2 . However, information on how to calculate target values from these NMR parameters in gases is scarce, especially for mixtures of gases. To enable detailed NMR studies of hydrogenation reactions, we investigated the T_1 relaxation of methane and hydrogen, which are two gases commonly present in hydrogenation reactions. To achieve industrially relevant conditions, the temperatures are varied from 290 to 600 K and the pressure from 1 bar to 5 bar, using different mixtures of methane and hydrogen. The results show that hydrogen, which is usually considered to be nondetectable in standard MRI sequences, can be measured at high concentrations, starting at a pressure of 3 bar even at temperatures above 400 K. In the investigated parameter range, the absolute T_1 values of hydrogen show only small dependence on temperature, pressure, and composition, while T_1 of methane is highly dependent on all three parameters. At a pressure of 5 bar, the measured values of T_1 for methane agree very well with theoretical predictions, so that they can also be used for temperature calculations. Further, it can be shown that the same measurement technique can be used to accurately calculate gas ratios inside each voxel. In conclusion, this study covers important aspects of spatially resolved *operando* NMR measurements of gas-phase properties during hydrogenation reactions at industrially relevant conditions to help improve chemical processes in the gas phase.

KEYWORDS: NMR, longitudinal relaxation time, heterogeneous catalysis, temperature measurements, Boltzmann distribution, temperature 290–600 K, pressure 1–5 bar (absolute)



1. INTRODUCTION

In chemical engineering, the process intensification of chemical reactions is one of the main tasks aiming to increase the efficiency of production steps.¹ Hydrogenation reactions are crucial in many chemical processes for the formation of specific products and in chemical energy storage.^{2,3} In many countries, the use of hydrogen moved more and more into focus, mainly as an energy source and as an energy carrier to decarbonize societies.^{4,5}

In this context, hydrogenation reactions are used to valorize carbon from different sources into chemicals or fuel. To boost the productivity of hydrogenation reactions, the efficiency of reaction systems (i.e., reactor and reacting conditions) should be optimized. An important factor here is the understanding of the macroscopic transport of heat, mass, and momentum in the reactor.⁶ Nuclear magnetic resonance (NMR) techniques offer numerous possibilities to spatially map process parameters of chemical reactions like velocities,^{7–11} mass transport,^{12,13} and

species distributions^{14,15} in opaque structures, *ex* and *in situ*, and even in the gas phase.

Prior NMR studies of the gas phase showed, however, that the detection of hydrogen gas using typical NMR sequences is very difficult or even impossible¹⁶ due to the high diffusion coefficient and short longitudinal and transversal relaxation times of hydrogen (D , T_1 , and T_2 , respectively). Furthermore, the presence of multiple gases (i.e., CH_4 , CO_2 , CO , H_2O) in varying concentrations during a chemical reaction poses a second challenge for *operando* measurements of heterogeneously catalyzed reactions. In a recent study,¹⁷ we were able to show that T_1 of methane offers information on the

Received: April 25, 2022

Revised: July 11, 2022

Accepted: July 11, 2022

Published: July 26, 2022



temperature of the gas, which we consider an important step toward the *operando* characterization of chemical reactions.

To tackle the obstacles of gas-phase NMR, in this work, we perform measurements of the longitudinal relaxation time T_1 of hydrogen and methane in mixtures of both gases. Similar mixtures are present in many hydrogenation reactions such as the Sabatier reaction and the Fischer–Tropsch synthesis. The measurements are performed using five different gas mixtures of hydrogen and methane (CH_4/H_2 ratios of 1:0, 1:3, 1:1, 3:1, and 0:1) and under industrially relevant conditions, with temperatures ranging from 290 K to approximately 600 K and pressures ranging from 1 to 5 bar (bar absolute). With these measurements, we elucidate the dependence of the T_1 of methane on temperature, pressure, and composition in the given temperature and pressure range and, more importantly, obtain a value for the effective cross section for the collision of methane with hydrogen, $\sigma_{j,\text{CH}_4-\text{H}_2}$, which has not been reported yet. This information is crucial to apply the existing theory of T_1 of methane in mixtures of methane and hydrogen. This allows thermometry experiments during hydrogenation reactions when mixtures of methane and hydrogen are present. Further, we show that the T_1 of hydrogen can be measured under certain pressure, temperature, and concentration conditions as well, which is noteworthy as hydrogen is usually considered to be undetectable using standard MRI sequences due to the time required for spatial encoding as well as low flip angles.^{16,18}

2. EXPERIMENTAL SECTION

2.1. Setup and Procedure

All measurements were carried out in a small cylindrical glass tube, which was open for gas flow at the top and bottom of the cylinder (Figure 1). The tube was positioned in the center of an NMR reactor, which was designed and built for high-temperature and -pressure applications; we have published details of this reactor in a previous paper.¹⁹ To heat up the tube, the unfocused but parallelized radiation of a 500 W diode laser was pointed directly on a black ceramic sponge positioned at the front of the tube inside the reactor (Figure 1, black sponge, and Appendix A, Figure A1). This way, only the sponge and, consequently, the tube was heated without the need to heat up the surrounding chemical reactor. This setup avoids high temperatures close to the NMR magnet and thus potential damage to the NMR magnet and radiofrequency (RF) coil as the heat is only absorbed inside the ceramic reactor. In a previous work, we already underlined the significance of thermal conductivity for radial heat removal in catalytic beds using CFD simulations.²⁰ The actual measurements of T_1 were carried out inside nonporous ceramic honeycomb structures positioned behind the black ceramic sponge. Using honeycombs ensures small radial temperature gradients inside the tube. The second honeycomb was used to offer a second temperature level for the measurement as the gap between the two monoliths interrupts thermal conduction. However, the gap further resulted in an inhomogeneous material distribution in between the two honeycombs, which compromised the quality of the measurements in the slices adjacent to the gap. Therefore, only the results of slices 9, 10, and 14 were used as indicated by the green areas in Figure 1. To fixate the three monoliths (one black sponge and two ceramic honeycombs) inside the glass tube, the last honeycomb was wrapped in fiberglass wool and fitted tightly into the tube.

For all measurements, we set a constant gas flow of $0.565 \text{ L}_\text{N}/\text{min}$ with changing gas composition. The pressure was measured after mixing the gases outside the NMR scanner's room and altered using a back-pressure regulator at the outlet of the chemical reactor. Each day was designated with one temperature level and one pressure level, with the gas composition varying over the day. At the start of the day,

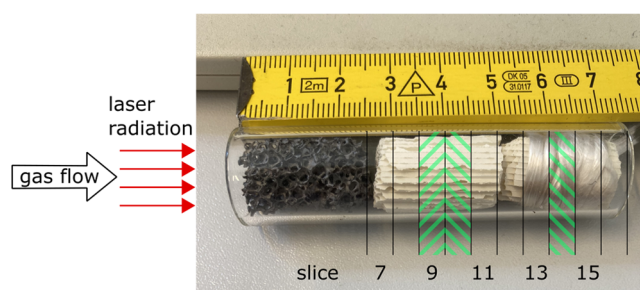


Figure 1. Picture of the cylindrical glass tube for the measurements with an inner diameter of 15 mm used for the NMR measurements. The unfocused but parallelized radiation of a diode laser was used to heat the tube (Appendix A). A black ceramic sponge at the front of the tube was used to absorb the laser radiation. The actual measurements of T_1 were carried out inside the two ceramic honeycomb structures. For the results, only slices 9, 10, and 14 were used as indicated by the green areas, as they yielded the highest magnetic field homogeneity (Appendix B). To fixate the three monoliths inside the glass tube, the last honeycomb was wrapped in fiberglass wool. The scale is in centimeters.

we measured pure methane at room temperature and at the designated pressure. Aside from being part of the measurement series, the initial measurement served as a reference for the temperature calculation using the amplitude ratio, as proposed in ref 17. After the initial measurement, we heated the system for approximately 90 minutes to reach a certain temperature level. The power level of the laser was kept constant each day. This way, the actual temperature inside the measurement tube changed only slightly as a function of gas composition and pressure. This was due to the different heat capacities of methane and hydrogen^{21,22} and the fact that methane partially absorbs the laser's radiation, while hydrogen does not. However, as the temperature was measured *operando* according to Eq. (3), these changes could be detected and were thus accounted for. We performed the measurements in an open system as this facilitated the change of gas composition and increased heat transport inside the tube. Further, open systems correspond to applications of heterogeneously catalyzed gas-phase reactions.

2.2. NMR Measurements

A 7 Tesla preclinical NMR imaging system (Biospec 70/20, Bruker Biospin GmbH, Ettlingen, Germany) equipped with a gradient system BGA12S2 (441 mT m^{-1} maximum gradient strength in each direction, $130 \mu\text{s}$ rise time) was used for all NMR measurements. A circularly polarized volume RF coil (inner diameter of 72 mm; MRI Tools GmbH, Berlin, Germany) was used for RF excitation and signal detection. The NMR pulse sequences were implemented using the software platform Paravision 5.1.

For the T_1 measurements, we used the same three-dimensional (3D) saturation recovery MRSI sequence described in our previous work.¹⁷ Using two 90° rectangular RF pulses each followed by spoiler gradients, the magnetization is reduced to a minimum and then, after a time τ , a third 90° rectangular RF pulse is used to flip the rebuilt magnetization again. Phase encoding gradients are applied in all three spatial directions (x , y , z) immediately after the third pulse, and the emerging free induction decay (FID) is acquired (FOV: $50 \text{ mm} \times 50 \text{ mm} \times 105 \text{ mm}$; matrix size: $25 \times 25 \times 21$ with an elliptically reduced k -space sampling). From each measurement, the 4D data set was fast Fourier-transformed in the three spatial dimensions and then fitted as a sum of exponentially decaying sinusoids in the time domain using the matrix pencil method (MPM).²³ The two signals of methane and hydrogen could be separated by their frequency difference of approximately 4.6 ppm. As a result of the fitting procedure, a series of amplitudes S per voxel (volume element) and per time value τ were acquired for methane and hydrogen gas individually. The data was fitted to the function

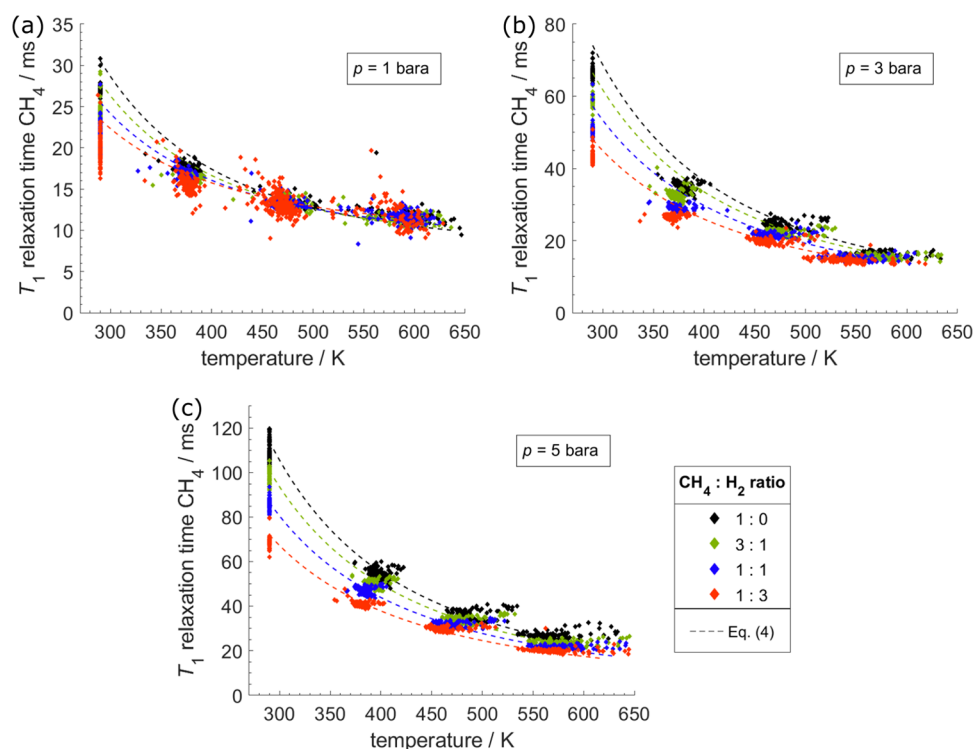


Figure 2. Longitudinal relaxation times T_1 of methane (CH_4) as a function of temperature and gas ratio at (a) $p = 1$ bara (ambient pressure), (b) $p = 3$ bara, and (c) $p = 5$ bara. One data point corresponds to a single evaluated voxel, resulting in $6 \times 6 \times 3$ data points per measurement. The temperature was calculated by the amplitude ratio from the voxel to its respective voxel measured at an ambient temperature and pure methane on the same day. Measurements at an ambient temperature are fixed at the standard temperature inside the scanner's room of 290 K.

$$S = A + (C - A)e^{-\tau/T_1} \quad (1)$$

using the “trust-region-reflective”-algorithm provided by MATLAB (mathworks.com, Version 2017b). The fitting parameters are the maximum signal amplitude A , the longitudinal relaxation time T_1 , and an error term C , which accounts for possible local deviations of the 90° flip angle, e.g., incomplete saturation.

One set of measurements was carried out at each of the four temperature levels (ambient temperature, ~ 370 K (20 W), ~ 470 K (40 W), and ~ 570 K (65 W)), three pressure levels (1 bara, 3 bara, and 5 bara), and five different gas ratios (CH_4/H_2 ratios of 1:0, 1:3, 1:1, 3:1, and 0:1). Thus, 60 different sets of measurements were performed in total. Each set consisted of 6–10 measurements using different values of τ . In the presence of methane, the maximum value of τ was always set to a value about three times the expected T_1 . The consecutive values of τ were then about halved each time to a minimum of 0.8 ms to get a proper reproduction of the exponential decay of the signal of methane. The same was done with hydrogen, but as the T_1 of hydrogen exhibits only slight absolute changes over the given parameter range, the τ values for hydrogen were kept constant (namely, 20, 12, 6, 3.5, 2, 0.8, and 0.5 ms). When both species were present, the choice of τ values was an amalgam of both ranges. The measurement time for a complete set increased almost linearly with the maximum τ value and increased from approximately 21 min at $\tau_{\text{max}} = 20$ ms to approximately 90 min at $\tau_{\text{max}} = 350$ ms. In each evaluated slice, the central 6×6 voxels were analyzed (nominal $12 \text{ mm} \times 12 \text{ mm}$ of the 15 mm diameter honeycombs). Results, alongside various measurement parameters, are given in a database available in a repository.²⁴ As mentioned before, only slices 9, 10, and 14 yielded sufficiently accurate results, as magnetic field inhomogeneities disturbed the proper measurement of temperature at each end of the honeycombs. This is further discussed in Appendix B.

To ensure temperature stability, consecutive slice-selective two-dimensional (2D) MRSI measurements (5 mm slice thickness in the x -direction, echo time 0.35 ms, repetition time 80 ms, 30° flip angle, no presaturation, 31×31 phase encoding steps using an elliptically

reduced k -space sampling, FOV 112 mm (z) \times 80 mm (y), 1024 complex data acquired with a spectral width of 50 kHz, ~ 5 min interval) were carried out prior to the actual 3D MRSI measurements described above. When the change in signal amplitude from one measurement to another was below 1%, the 3D MRSI measurements were started. However, the ratio of two subsequent signal amplitudes could only be determined for methane. Further, when the gas concentration of methane was low, either due to low pressure or low methane gas ratios, the technique failed as the signal variance was too high. In this case, the waiting time was determined from experience from prior measurements.

The temperature was calculated for each voxel using the temperature dependence of the signal amplitude A in comparison to the signal amplitude A_0 at room temperature T_0 , which was also proposed in our previous work¹⁷

$$A = A_0 \frac{T_0 \rho_i}{T \rho_{i,0}} \quad (2)$$

The equation was adapted to the open system with changing pressure and gas composition replacing the average molecular gas density ρ by the pressure p and molar concentration of methane x_{CH_4} , using the ideal gas law and Dalton's law

$$T = T_0 \frac{A_0 \rho}{A \rho_0} = T_0 \left(\frac{A_0 p x_{\text{CH}_4}}{A p_0 x_{\text{CH}_4,0}} \right)^{1/2}$$

with $\rho_i = \frac{p_i}{RT}$, $p_{\text{CH}_4} = p x_{\text{CH}_4}$

$$T_0 = 290 \text{ K and } x_{\text{CH}_4,0} = 1 \quad (3)$$

The T_1 measurements of methane are compared to the equation proposed by Dong and Bloom²⁵ and Beckmann²⁶

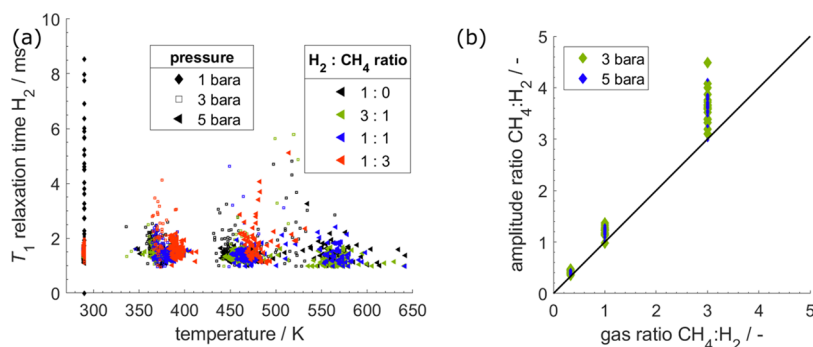


Figure 3. (a) Longitudinal relaxation times T_1 of hydrogen (H_2) at different temperatures, pressures, and gas ratios. One data point corresponds to a single evaluated voxel, resulting in $6 \times 6 \times 3$ data points per measurement. The temperature was calculated by the amplitude ratio of methane from the voxel to its respective voxel measured at an ambient temperature and pure methane on the same day. For the pure hydrogen measurements, the temperature was extrapolated from the temperatures of the other measurements at the same pressure and laser heating level. Measurements at an ambient temperature are fixed at the standard temperature inside the scanner's room of 290 K. (b) Ratio of signal amplitude from methane and hydrogen T_1 measurements over the applied gas ratio (CH_4/H_2). At $p = 1$ bara, no hydrogen signal could be detected in gas mixtures due to low SNR. The data points of the 3 bara measurements have been enlarged for better visibility.

$$T_1^{-1} = \frac{4\pi^2}{\hbar^2} C_{\text{eff}}^2 2I_0 k_B T \frac{\tau_1}{1 + (\omega_0 - \omega_L)^2 \tau_1^2} \quad (4)$$

Here, $\hbar = 1.0546 \times 10^{-34}$ J s is the reduced Planck constant, C_{eff}^2 is calculated similar to our previous work,¹⁷ the effective spin-rotation constant, $I_0 = 5.33 \times 10^{-47}$ kg m² is the principal moment of inertia of methane, $k_B = 1.3806 \times 10^{-23}$ J K⁻¹ is the Boltzmann constant, T is the temperature, τ_1 is the average time between molecular collisions, $\omega_0/2\pi = 300$ MHz is the nuclear Larmor frequency, and $\omega_L/2\pi = 16.8$ MHz is the rotational frequency.

The average time between molecular collisions $\tau_1^{-1} = \bar{v}\rho\sigma_j$ is calculated using the mean relative gas velocity \bar{v} , the average molecular gas density ρ , and the effective cross section σ_j . The theory was previously applied mostly to pure methane gas, but both \bar{v} and σ_j are dependent on the colliding molecule, which in the case of our mixture can either be hydrogen or methane. For such a mixture, τ_1^{-1} is calculated as the sum of the molecular density of species i multiplied by the effective cross section for the collision of methane with species i , σ_{j,CH_4-i} and their mean relative gas velocity \bar{v}_{CH_4-i} ²⁷

$$\tau_1^{-1} = \bar{v}\rho\sigma_j \xrightarrow{\text{mixtures}} \tau_1^{-1} = \sum_{i=1}^n \tau_{1,CH_4-i}^{-1}$$

$$\tau_1^{-1} = \sum_{i=1}^n \bar{v}_{CH_4-i} \rho_i \sigma_{j,CH_4-i} \quad (5)$$

While the cross sections for the collision of methane with many different gas species were already determined by Jameson et al.,²⁸ the cross section for the collision of methane with hydrogen σ_{j,CH_4-H_2} was not reported yet. We will therefore determine the parameter in this work.

3. RESULTS AND DISCUSSION

3.1. T_1 Relaxation of Methane

In this section, we show the results of the T_1 relaxation of methane to elaborate how gas-phase hydrogenation reactions can be described *operando*. Longitudinal relaxation times T_1 as a function of temperature for different pressures and gas ratios are shown in Figure 2. Each panel contains the results of one pressure level. T_1 -values calculated from the theory (eq 4) are also plotted. The required collision cross section σ_{j,CH_4-H_2} was unknown a priori; we have therefore extracted this parameter by fitting eq 4 to the experimentally determined T_1 at all mixture compositions and temperatures and at the highest pressure level of 5 bara. The collision cross section for

methane–methane collisions was taken from Jameson et al.²⁸ as $\sigma_{j,CH_4-CH_4} = 18.4 (T/300 \text{ K})^{-0.9} \text{ \AA}^2$.

At $p = 1$ bara (Figure 2a), the theory predicts little dependence of T_1 on gas composition (lines). The measurements show a high statistic uncertainty, making it virtually impossible to distinguish between different gas compositions. The temperature dependence of T_1 , which is visible from the theory, is obstructed by the uncertainty in the measurement. The results manifest the findings of our previous publication,¹⁷ where we measured the temperature of pure methane in a sealed tube at approximately 0.9 bara and found an equally high uncertainty. However, it can be seen from Figure 2a that at low temperatures the theoretically predicted T_1 relaxation times are higher than the measured values.

At $p = 3$ bara, T_1 shows a clear dependence on the gas ratio both in theory and from the experimental data (Figure 2b). T_1 increases with the methane-to-hydrogen ratio but decreases with temperature. In comparison to 1 bara, the temperature dependence is more pronounced and experiments show only little statistic uncertainty. However, similar to 1 bara, the theoretical T_1 -values are higher than the measured T_1 -values at lower temperatures. A possible reason for the overestimation might be our model for C_{eff} which is deployed on the basis of data by Beckmann²⁶ who used a Larmor frequency of $\omega_0/2\pi = 30$ MHz. The model might thus be insufficient to properly reproduce data at the Larmor frequency used in this study, $\omega_0/2\pi = 300$ MHz. A second common mechanism for the reduction of T_1 is wall interaction.²⁹ However, we were able to reproduce the measured values of T_1 at an ambient temperature in a gas sampling container with a large diameter (approximately 60 mm) made of glass where no wall interaction can be expected. As the overestimation only arises toward lower temperatures but wall interaction should increase with increasing temperature, the effect of wall interaction with the used honeycombs is neglected.

At $p = 5$ bara (Figure 2c), the dependence of T_1 on temperature and concentration is even more pronounced and the uncertainty is reduced further. Here, eq 4 is able to reproduce the data points accurately over all measured temperatures. Therefore, we extracted the parameter σ_{j,CH_4-H_2} by fitting eq 4 to this measurement series. As mentioned before, the parameter is required for theoretical predictions of

T_1 of methane in the presence of hydrogen. From a linear least-squares fit to all data points of methane/hydrogen mixtures at $p = 5$ bara, the effective cross section for the collision of methane with hydrogen was determined as $\sigma_{i,\text{CH}_4-\text{H}_2} = (4.07 \pm 0.09) (T/300 \text{ K})^{-(0.52 \pm 0.01)} \text{ \AA}^2$ (uncertainty given as 95% confidence interval) using the same temperature-dependent approach for σ_j as Jameson et al.²⁸ This parameter was then used for the theoretical curves at all pressures in Figure 2.

The T_1 relaxation of methane decreases with increasing hydrogen concentration because the cross section $\sigma_{i,\text{CH}_4-\text{H}_2}$ is lower than $\sigma_{i,\text{CH}_4-\text{CH}_4}$. At constant pressure and temperature, a higher hydrogen concentration results in a smaller average collision probability and thus a higher time between collisions τ_1 . In the extreme narrowing limit ($(\tau_1\omega)^2 \ll 1$), this results in smaller T_1 relaxation times, as can be derived from eq 4.

3.2. T_1 Relaxation of Hydrogen

This section extends the measurements of T_1 relaxation times to hydrogen and, thus, demonstrates that in a certain parameter range hydrogen gas is detectable using 3D MRSI. The results of the T_1 relaxation times are shown in Figure 3a. The T_1 of hydrogen changes only slightly in the investigated parameter range. Therefore, the results are summarized in a single plot. For hydrogen, only the seven lowest values of τ are used because at higher values the signal of methane was more likely to overshadow the signal of hydrogen, which compromised the quality of the fit of eq 1. The temperature was taken from the methane measurement of the same voxel and, in the case of pure hydrogen, linearly extrapolated over the change in density. No dependence of T_1 on temperature, pressure, or gas ratio can be observed as the results are obscured by the high amount of uncertainty. Other works found a T_1 relaxation time of hydrogen of 3.1 ms¹⁶ (1 bara, room temperature, 299 MHz) and 3.7 ms³⁰ (1 bara, room temperature, 500 MHz), which are in the same range as the obtained data. Extrapolating the data shown by Lalita et al.³¹ to the pressure range of our study leads to much shorter T_1 values. However, it is important to note that this study was performed at 30 MHz and higher pressure ($p \geq 7$ bar). Armstrong³² compared $T_1(p)$ data for hydrogen at 77.5 K measured at different NMR frequencies, which illustrates the shift of the T_1 minimum to higher density and higher T_1 values with increasing NMR frequency. From this data, one can estimate that our measurements at 300 MHz and the investigated parameter range of temperature, concentration, and pressure were performed near the T_1 minimum. Thus, besides the limited data quality, this fact might explain why no significant changes in the T_1 relaxation time of hydrogen could be detected in our study.

At $p = 1$ bara, T_1 data could only be calculated at room temperature, and for pure hydrogen, as at increased temperatures and in mixtures, no hydrogen signal could be detected. We also did not detect a hydrogen signal at a H_2/CH_4 ratio of 1:3 at $p = 3$ bara and $T \approx 480$ K and at $p = 5$ bara and $T \approx 580$ K. Even though no reliable information on exact T_1 relaxation times of hydrogen can be derived from the given data, Figure 3a illustrates the range in which T_1 measurements of hydrogen can be performed.

The uncertainty can partly be explained by the low SNR of hydrogen in general, as well as the low amount of signal compared to methane. The observed T_2^* of hydrogen (which we share in our repository²⁴) ranges from about 0.3 to 1 ms.

Therefore, at the beginning of data acquisition, after a time delay T_D of 300 μs , about 63–26% of the observable transverse magnetization was already lost before data acquisition started ($S \sim \exp(-T_D/T_2^*)$), which drastically reduced the SNR. In most MRI and MRSI sequences, T_D has a duration of 1 ms and longer, which might explain why in these studies hydrogen seemed to be undetectable. The methane molecule contains twice as many protons as the hydrogen molecule. As a result, when the same amount of hydrogen and methane is present, the signal amplitude of hydrogen is always by a factor of 1/2 smaller, which further reduces the signal intensity of hydrogen gas.

3.3. Determination of Gas Ratio

In the previous sections, the T_1 relaxation of mixtures of methane and hydrogen was evaluated. By fitting eq (1) to a set of τ values, we can derive not only T_1 but also the maximum signal amplitude of each species, A . As shown before,¹⁸ the amplitude ratio of two gas signals inside a single voxel is proportional to the ratio of molecules in the same volume.

From this, using *a priori* knowledge of input gas composition and stoichiometry, we can eventually calculate the gas concentration. This is favorable, as for ideal gases, the ratio is independent of the applied pressure and temperature. For chemical reactions in which hydrogen participates as a reactant and methane as a product—such as the Sabatier reaction ($\text{CO}_2 + 4 \text{H}_2 \rightleftharpoons \text{CH}_4 + 2\text{H}_2\text{O}$)—this information can be vital to characterize local yields and accurate temperature information.

Amplitude ratios calculated from the results of this study are shown in Figure 3b as a function of the applied gas ratio. The signal amplitudes have been extrapolated to the time of excitation (300 μs prior to data acquisition). Voxels in which the phase difference between methane and hydrogen at excitation was larger than 0.05π were considered bad fits and subsequently omitted. As hydrogen could not be quantified in a gas mixture at $p = 1$ bara, only data for 3 bara and 5 bara is shown.

The amplitude ratio follows the applied gas ratio very well. However, the amplitude ratios are on average 16% higher than the gas ratios. A systematic deviation of input gas ratios is negligible, as mass flow controllers were checked using a bubble flow meter. A possible cause for the deviation could be the fast signal decay of hydrogen due to its low T_2^* . As a result, the methane signal dominates the acquired FID data, which might lead to an overestimation of the methane signal (see Figure B1 of Appendix B). As stated before, because of the smaller number of hydrogen nuclei per molecule and the much shorter T_2^* values, the SNR of hydrogen is lower than that of methane. This might explain why the uncertainty of the method increases with the CH_4/H_2 ratio, as only a very poor SNR of hydrogen remains. Furthermore, the assumed Lorentzian signal decay does not perfectly describe the measured FIDs (see Figure C1 of Appendix C1). As we extrapolate the signal decay to calculate the gas ratios, the fitting error increases as well.

4. CONCLUSIONS

In this work, we measured the longitudinal relaxation times T_1 of mixtures of hydrogen and methane at different pressures from 1 to 5 bara, temperatures from 290 to approximately 580 K, and at different gas ratios. T_1 of methane decreased with the temperature at all investigated pressures, as predicted by the theory. At lower pressures, 1 bara and 3 bara, and temperatures

<400 K, the measured values of T_1 are smaller than expected by the theory. At 5 bara, experimental results and theory match very well; thus, the data was used to estimate the effective cross-sectional parameter $\sigma_{j,\text{CH}_4+\text{H}_2}$, which is required to expand the theory to be able to predict T_1 of methane in mixtures with hydrogen, which is a common scenario in hydrogenation reactions. In the range $p \geq 5$ bara, the theoretical prediction can then be used to calculate gas-phase parameters like concentration or temperature, as shown in our previous work.¹⁷

From our obtained data as well as theory, we showed that toward higher temperatures T_1 of methane at 1 bara only slightly depends on gas ratio, while the dependence of T_1 on gas ratio at 3 and 5 bara is more pronounced. Furthermore, the uncertainty of the results is significantly lower at 3 and 5 bara than at 1 bara. Both these results demonstrate the importance of carrying out NMR measurements of the gas phase at pressures above ambient. An increase of pressure to 3 bara already has a significant influence on the measurement quality. Increasing the pressure further might allow us to decrease the voxel size from the quite large nominal $2 \text{ mm} \times 2 \text{ mm} \times 5 \text{ mm}$ to achieve a finer spatial resolution. However, this comes with a significant increase in measurement time, as higher pressures result in a larger T_1 of methane, which requires higher τ values to be measured properly. This would add up on top of the increase in measurement time caused by the larger number of phase encoding steps required for a higher spatial resolution at a fixed field of view.

Additionally, we were able to measure T_1 of hydrogen under temperature and pressure conditions relevant to chemical reactions. The success of the spatially resolved detection of hydrogen gas is mainly due to the use of an MRSI sequence with a short time delay T_D of only 300 μs . Furthermore, only short rectangular RF pulses are used in this 3D MRSI sequence to avoid a prolonged echo time and signal damping by diffusion weighting caused by slice-selection gradients. A general drawback of this approach is that a rather large FOV is required, which covers the whole volume from which NMR signals are detected by the RF reception coil. This leads to a long minimum total measurement time for a given voxel size. However, a considerably shorter total measurement time would not be adequate for many quantitative studies because the inherently low SNR of gas-phase NMR studies would require signal averaging.

To map the spatial distribution of hydrogen gas by NMR techniques, it is of the highest importance to increase SNR either by increasing the pressure or by reducing the ratio between the time delay for switching gradients T_D and T_2^* . While T_D is limited by the hardware of the gradient coil, T_2^* is heavily affected by material properties in the region of interest. Optimizing these two parameters will be a challenge for MRSI measurements of hydrogen.

From the fitting of T_1 , the maximum signal amplitude can be estimated, which, when enough hydrogen is present, can be used to calculate the gas ratio of methane and hydrogen in a single voxel. This is suited for the application of hydrogenation reactions, as the gas ratio is independent of pressure and temperature. For many hydrogenation reactions, a high percentage of hydrogen is fed into the reactor as it not only reacts with new hydrocarbon species but is also required to bind excess oxygen, e.g., carbon mono- or dioxide. Thus, a high

hydrogen/product ratio could benefit the NMR measurement and result in a higher accuracy of the measurement.

Apart from adding new measured NMR parameters to the record, the current work elucidates important aspects required to perform spatially resolved *operando* measurements of gas-phase reactions under industrially relevant conditions. To achieve good accuracy, especially at higher temperatures, a pressure above 3 bara is required. To detect hydrogen, the echo time must be kept as short as possible and a pressure of ≥ 5 bara should be applied to accurately apply the theory on T_1 of methane to calculate gas-phase parameters like temperature. We consider the findings of this work to be crucial in the development of new NMR methods to study gas-phase reactions involving methane and hydrogen. With precise knowledge about the relaxation times of each different species, NMR sequences can be tailored to create image contrast of specific parameters and give new insight into reaction systems.

■ ASSOCIATED CONTENT

SI Supporting Information

The Supporting Information is available free of charge at <https://pubs.acs.org/doi/10.1021/acsmesuresciau.2c00022>.

Appendix A describes the used diode laser setup that was used for heating the glass tube; Appendix B briefly elucidates the signal separation using the MPM fitting procedure; and in Appendix C, an example of the influence of the object geometry on the line shape is given (PDF)

■ AUTHOR INFORMATION

Corresponding Author

Harm Ridder – Chemical Process Engineering (CVT), Faculty of Production Engineering, University of Bremen, 28359 Bremen, Germany; Center for Environmental Research and Sustainable Technology (UFT), 28334 Bremen, Germany; orcid.org/0000-0002-5894-849X; Email: harm.ridder@uni-bremen.de

Authors

Christoph Sinn – Chemical Process Engineering (CVT), Faculty of Production Engineering, University of Bremen, 28359 Bremen, Germany; Center for Environmental Research and Sustainable Technology (UFT), 28334 Bremen, Germany; orcid.org/0000-0002-4425-4788

Georg R. Pesch – Chemical Process Engineering (CVT), Faculty of Production Engineering, University of Bremen, 28359 Bremen, Germany; Center for Environmental Research and Sustainable Technology (UFT), 28334 Bremen, Germany; MAPEX Center for Materials and Processes, University of Bremen, 28334 Bremen, Germany; orcid.org/0000-0003-4676-1908

Wolfgang Dreher – *in vivo* MR group, Faculty of Chemistry, University of Bremen, 28359 Bremen, Germany; orcid.org/0000-0001-5132-6834

Jorg Thöming – Chemical Process Engineering (CVT), Faculty of Production Engineering, University of Bremen, 28359 Bremen, Germany; Center for Environmental Research and Sustainable Technology (UFT), 28334 Bremen, Germany; MAPEX Center for Materials and Processes, University of Bremen, 28334 Bremen, Germany; orcid.org/0000-0002-5374-114X

Complete contact information is available at:
<https://pubs.acs.org/10.1021/acsmeasuresci.2c00022>

Author Contributions

H.R. conceived of the study, designed and assembled the experimental setup, designed the postprocessing procedure, wrote the GUI for postprocessing, carried out data analysis, and drafted the manuscript; C.S. participated in the design of the study, participated in the assembly of the experimental setup, and critically revised the manuscript; G.P. participated in the design of the study and critically revised the manuscript; W.D. participated in the design of the study, designed and tested the used saturation recovery sequence, performed NMR measurements, and critically revised the manuscript; and J.T. coordinated the study and critically revised the manuscript. All authors gave final approval for publication and agreed to be held accountable for the work performed therein. CRediT: **Harm Ridder** data curation (equal), investigation (equal), methodology (lead), software (lead), validation (equal), visualization (lead), writing-original draft (lead), writing-review & editing (supporting); **christoph sinn** conceptualization (supporting), validation (supporting), writing-original draft (supporting), writing-review & editing (supporting); **Georg R. Pesch** conceptualization (supporting), supervision (supporting), visualization (supporting), writing-original draft (supporting), writing-review & editing (equal); **Wolfgang Dreher** conceptualization (supporting), data curation (equal), formal analysis (equal), methodology (supporting), resources (equal), software (equal), supervision (supporting), validation (lead), writing-original draft (supporting), writing-review & editing (supporting); **Jorg Thöming** funding acquisition (lead), project administration (lead), supervision (lead), writing-original draft (supporting), writing-review & editing (supporting).

Notes

The authors declare no competing financial interest. A database with the collected T_1 relaxation data of hydrogen and methane at varying pressures, temperatures, and gas ratios is available in the given repository.²⁴ The database is given as the MATLAB readable file and as an open source data format. Further, the repository contains the raw data of the performed series of NMR experiments as well as the MATLAB script and GUI used for postprocessing.

ACKNOWLEDGMENTS

This work was developed in the context of the research project “QUARREE 100—Resilient, integrated and system-friendly energy supply systems in existing urban districts considering the complete integration of renewable energies” (grant number: 03SBE113B). The authors thank the project management organisation Jülich (PtJ), the Federal Ministry for Economic Affairs and Energy (BMWi), and the Federal Ministry of Education and Research (BMBF).

LIST OF SYMBOLS

Roman

A	signal amplitude, a.u.
C_{eff}	effective spin-rotation constant, Hz
D	diffusion coefficient, $\text{m}^2 \text{s}^{-1}$
\hbar	reduced Planck constant, J s
$\Delta_{\text{r}}H^{298\text{K}}$	standard enthalpy of reaction, J mol ⁻¹

I_0	principal moment of inertia, kg m^2
k_{B}	Boltzmann constant, J K^{-1}
p	pressure, Pa
R	molar gas constant, $\text{J K}^{-1} \text{mol}^{-1}$
S	signal intensity, a.u.
T	temperature, K
T_1	longitudinal relaxation time, s
T_2	transversal relaxation time, s
T_2^*	effective transversal relaxation time, s
T_D	time delay, s
\bar{v}	mean relative gas velocity, m s^{-1}
x	molar concentration

GREEK

σ_j	effective cross section for the collision of two molecules, m^2
ρ	average molecular density, mol m^{-3}
τ	time between the second and third 90°-flip-pulses, s
τ_1	average time between molecular collisions, s
ω_0	nuclear Larmor frequency, Hz
ω_{L}	rotational frequency, Hz

REFERENCES

- Grützner, T.; Ziegenbalg, D.; Güttel, R. Process Intensification – An Unbroken Trend in Chemical Engineering. *Chem. Ing. Tech.* **2018**, *90*, 1823–1831.
- Jorschick, H.; Preuster, P.; Bösmann, A.; Wasserscheid, P. Hydrogenation of aromatic and heteroaromatic compounds—a key process for future logistics of green hydrogen using liquid organic hydrogen carrier systems. *Sustainable Energy Fuels* **2021**, *5*, 1311–1346.
- Dieterich, V.; Buttler, A.; Hanel, A.; Spliethoff, H.; Fendt, S. Power-to-liquid via synthesis of methanol, DME or Fischer–Tropsch-fuels: a review. *Energy Environ. Sci.* **2020**, *13*, 3207–3252.
- Nagashima, M. Japan’s hydrogen strategy and its economic and geopolitical implications *Études de l’Ifri*. 2018, p 75 https://www.ifri.org/sites/default/files/atoms/files/nagashima_japan_hydrogen_2018_.pdf (accessed July 5, 2022).
- Cuevas, F.; Zhang, J.; Latroche, M. The Vision of France, Germany, and the European Union on Future Hydrogen Energy Research and Innovation. *Engineering* **2021**, *7*, 715–718.
- Gascon, J.; Van Ommen, J. R.; Moulijn, J. A.; Kapteijn, F. Structuring catalyst and reactor - An inviting avenue to process intensification. *Catal. Sci. Technol.* **2015**, *5*, 807–817.
- Sadeghi, M.; Mirdrikvand, M.; Pesch, G. R.; Dreher, W.; Thöming, J. Full-field analysis of gas flow within open-cell foams: comparison of micro-computed tomography-based CFD simulations with experimental magnetic resonance flow mapping data. *Exp. Fluids* **2020**, *61*, No. 124.
- Onstad, A. J.; Elkins, C. J.; Medina, F.; Wicker, R. B.; Eaton, J. K. Full-field measurements of flow through a scaled metal foam replica. *Exp. Fluids* **2011**, *50*, 1571–1585.
- Kemper, P.; Küstermann, E.; Dreher, W.; Helmers, T.; Mießner, U.; Besser, B.; Thöming, J. Magnetic Resonance Imaging for Non-invasive Study of Hydrodynamics Inside Gas-Liquid Taylor Flows. *Chem. Eng. Technol.* **2021**, *44*, 465–476.
- Galvosas, P.; Callaghan, P. T. Fast magnetic resonance imaging and velocimetry for liquids under high flow rates. *J. Magn. Reson.* **2006**, *181*, 119–125.
- Penn, A.; Boyce, C. M.; Pruessmann, K. P.; Müller, C. R. Regimes of jetting and bubbling in a fluidized bed studied using real-time magnetic resonance imaging. *Chem. Eng. J.* **2020**, *383*, No. 123185.
- D’Agostino, C.; Brett, G. L.; Miedziak, P. J.; Knight, D. W.; Hutchings, G. J.; Gladden, L. F.; Mantle, M. D. Understanding the solvent effect on the catalytic oxidation of 1,4-butanediol in methanol

over Au/TiO₂ catalyst: NMR diffusion and relaxation studies. *Chem. – Eur. J.* **2012**, *18*, 14426–14433.

(13) Isaacs, M. A.; Robinson, N.; Barbero, B.; Durndell, L. J.; Manayil, J. C.; Parlett, C.M.A.; D'Agostino, C.; Wilson, K.; Lee, A. F. Unravelling mass transport in hierarchically porous catalysts. *J. Mater. Chem. A* **2019**, *7*, 11814–11825.

(14) Ulpts, J.; Kiewidt, L.; Dreher, W.; Thöming, J. 3D characterization of gas phase reactors with regularly and irregularly structured monolithic catalysts by NMR imaging and modeling. *Catal. Today* **2018**, *310*, 176–186.

(15) Baker, L.; Renshaw, M. P.; Mantle, M. D.; Sederman, A. J.; Wain, A. J.; Gladden, L. F. Operando Magnetic Resonance Studies of Phase Behaviour and Oligomer Accumulation Within Catalyst Pores During Heterogeneous Catalytic Ethene Oligomerization. *Appl. Catal. A Gen.* **2018**, *557*, 125–134.

(16) Koptuyug, I. V.; Altobelli, S. A.; Fukushima, E.; Matveev, A. V.; Sagdeev, R. Z. Thermally Polarized ¹H NMR Microimaging Studies of Liquid and Gas Flow in Monolithic Catalysts. *J. Magn. Reson.* **2000**, *147*, 36–42.

(17) Ridder, H.; Sinn, C.; Pesch, G. R.; Dreher, W.; Thöming, J. Spatially resolved direct gas-phase thermometry in chemical reactors using NMR. *Chem. Eng. J.* **2022**, *433*, No. 133583.

(18) Ulpts, J.; Dreher, W.; Kiewidt, L.; Schubert, M.; Thöming, J. In situ analysis of gas phase reaction processes within monolithic catalyst supports by applying NMR imaging methods. *Catal. Today* **2016**, *273*, 91–98.

(19) Ridder, H.; Sinn, C.; Pesch, G. R.; Ilsemann, J.; Dreher, W.; Thöming, J. A large fixed bed reactor for MRI operando experiments at elevated temperature and pressure. *Rev. Sci. Instrum.* **2021**, *92*, No. 043711.

(20) Sinn, C.; Wentrup, J.; Pesch, G. R.; Thöming, J.; Kiewidt, L. Structure-heat transport analysis of periodic open-cell foams to be used as catalyst carriers. *Chem. Eng. Res. Des.* **2021**, *166*, 209–219.

(21) Methane - NIST Chemistry WebBook, *Natl. Inst. Stand. Technol.* <https://webbook.nist.gov/cgi/cbook.cgi?ID=C74828> (accessed July 5, 2022).

(22) Hydrogen - NIST Chemistry WebBook, *Natl. Inst. Stand. Technol.* <https://webbook.nist.gov/cgi/cbook.cgi?ID=C1333740> (accessed July 5, 2022).

(23) Lin, Y. Y.; Hodgkinson, P.; Ernst, M.; Pines, A. A Novel Detection-Estimation Scheme for Noisy NMR Signals: Applications to Delayed Acquisition Data. *J. Magn. Reson.* **1997**, *128*, 30–41.

(24) Ridder, H. Repository for “T1 relaxation of methane/hydrogen mixtures for operando characterization of chemical reactions. *Zenodo. Org.* **2022**, DOI: 10.5281/zenodo.6670098.

(25) Dong, R. Y.; Bloom, M. Determination of spin-rotation interaction constants in fluorinated methane molecules by means of nuclear spin relaxation measurements. *Can. J. Phys.* **1970**, *48*, 793–804.

(26) Beckmann, P. A. Nuclear Spin Relaxation in Methane Gas. PhD [dissertation]; University of British Columbia, 1975.

(27) Gordon, R. G. Kinetic theory of nuclear spin relaxation in gases. *J. Chem. Phys.* **1966**, *44*, 228–234.

(28) Jameson, C. J.; Jameson, A. K.; Smith, N. C.; Hwang, J. K.; Zia, T. ¹³C and ¹H spin relaxation in CH₄ in the gas phase. *J. Phys. Chem. A* **1991**, *95*, 1092–1098.

(29) Bardenhagen, I.; Dreher, W.; Fenske, D.; Wittstock, A.; Bäumer, M. Fluid distribution and pore wettability of monolithic carbon xerogels measured by ¹H NMR relaxation. *Carbon* **2014**, *68*, 542–552.

(30) Gamliel, A.; Allouche-Armon, H.; Nalbandian, R.; Barzilay, C. M.; Gomori, J. M.; Katz-Brull, R. An Apparatus for Production of Isotopically and Spin-Enriched Hydrogen for Induced Polarization Studies. *Appl. Magn. Reson.* **2010**, *39*, 329–345.

(31) Lalita, K.; Bloom, M.; Noble, J. D. Nuclear spin relaxation in hydrogen gas. *Can. J. Phys.* **1969**, *47*, 1355–1369.

(32) Armstrong, R. L. Longitudinal Nuclear Spin Relaxation Time Measurements in Molecular Gases. *Introd. Essays* **1976**, 71–95.